AGU
ADVANCING EARTH AND SPACE SCIENCE

Geophysical Research Letters®

Can Convective Cold Pools Lead to the Development of Low-Level Jets?

E. W. Luiz[1] and **S. Fiedler[1,2,3]**

[1]Institute for Geophysics and Meteorology, University of Cologne, Cologne, Germany, [2]Now at GEOMAR Helmholtz Centre for Ocean Research Kiel, Kiel, Germany, [3]Now at Faculty for Mathematics and Natural Sciences, Kiel University, Kiel, Germany

Abstract We present the first observational evidence for convectively generated cold pools (CP) as driving mechanism for low-level jets (LLJ). Our findings are based on a unique campaign data set that allowed us to perform a systematic assessment of the process. During the three-month campaign in Germany, 6.8% of all identified LLJ profiles were connected to a CP (CPLLJ). Most measured CPLLJs appeared with the CP front and lasted for up to two hours. Moreover, we have observed a CP favoring the formation of a several-hours long LLJ. In that case, a strong LLJ and cooling of the atmosphere between the surface and at least 400 m a.g.l. were seen when the density current reached the measurement site. The development led to the formation of a near-surface temperature inversion during daytime as a prerequisite for the LLJ, not unlike the mechanism of nocturnal LLJs.

Plain Language Summary Low-level jets (LLJ) are strong winds that occur in the lowest few hundred meters of the atmosphere. Their influence ranges from transporting moisture and pollutants, to impacts on aviation safety and wind power production. LLJs typically occur at night, when the surface strongly cools, for example, during cloud-free skies. Newly available measurement data from a campaign in summer 2021 gives us the unique opportunity to test the hypothesis that LLJs can also be driven by convectively generated cold pools (CPs). CPs are areas of relatively cool and dense air formed by downdrafts underneath precipitating clouds. Our study provides the first observational evidence that CPs can favor the generation of a temperature inversion, with reduced friction of the winds with the surface, as a prerequisite for generating LLJs also during daytime. The observations show how CPs and LLJs are connected to each other.

1. Introduction

Low-level jets (LLJ) are wind speed maxima in the lowest 50–500 m of the troposphere (e.g., Shapiro & Fedorovich, 2010; Ziemann et al., 2020). They have implications for the transport of moisture and pollutants (e.g., Angevine et al., 2006; R. Chen & Tomassini, 2015), for aviation safety (e.g., Blackadar, 1957), the formation of dust storms (e.g., Schepanski et al., 2009), and wind power production (e.g., Gutierrez et al., 2016; Lampert et al., 2016). In the classical theoretical description of inertial oscillations, LLJs develop due to the decoupling of nocturnal winds from the surface friction by the formation of a near-surface temperature inversion (Blackadar, 1957; Van de Wiel et al., 2010). These conditions typically occur at night, particularly during cloud-free conditions that allow strong radiative cooling of the surface (Beyrich, 1994; Sisterson & Frenzen, 1978). LLJs formed by this mechanism are often called Nocturnal LLJs (NLLJ).

Other driving mechanisms for LLJs are known. A LLJ can form when a near-surface temperature inversion is formed by warm air advection over relatively cooler near-surface air. The associated tilt of isobaric surfaces leads to a thermal wind that under certain conditions can manifest itself as a LLJ. LLJs have been also connected to synoptic scale systems (G. T.-J. Chen et al., 2006; Li & Du, 2021; Corrêa et al., 2021) and cols pools. Cold pools are mesoscale areas of relatively cool and dense air, which can be formed as a consequence of cold air drainage toward lower terrain in calm wind conditions confined by topography (Whiteman et al., 2001) or convectively generated through downdrafts associated with evaporation of hydrometeors underneath precipitating clouds (Drager & van den Heever, 2017). While the former was well connected to LLJs (e.g., R. M. Banta et al., 2004; Lu & Zhong, 2014), the connection between convectively generated cold pools (CPs) and LLJs was only analyzed in kilometer-scale regional model simulations partially resolving convective processes (Heinold et al., 2013). According to Heinold et al. (2013), the LLJ profiles are generated by aged CPs from deep

convective clouds that glide up over a radiatively generated stable near-surface layer, which was not simulated by a convection-parameterizing regional model. Up to date there was no systematic assessment of CPs as driving mechanism for LLJs due to the lack of suitable observational data. We now have the opportunity to overcome these observational limits by combining different measurements that were collected during a unique campaign in summer 2021 (FESSTVaL, Hohenegger et al.,). Specifically, we use the new data set to test the hypothesis that LLJs can be driven by CPs and that this is due to their cooling effect on the near-surface layer itself.

2. Data and Methods

2.1. FESSTVal Campaign

This study is based on data from the Field Experiment on Submesoscale Spatio-Temporal Variability (FESST-VaL, Hohenegger et al.,). The primary goal of FESSTVaL is measuring sub-mesoscale to mesoscale variability employing a measurement strategy to cover three main aspects: boundary layer patterns, convective cold pools and wind gusts. The FESSTVaL campaign took place from June to August 2021 in the region of the Meteorological Observatory Lindenberg–Richard Assmann Observatory (MOL-RAO) of the German Weather Service (DWD). MOL-RAO is situated in a rural area of the federated state Brandenburg in Eastern Germany (EG). The campaign was special due to a dense network for near-surface measurements, with 82 low-cost APOLLO (Autonomous cold POoL LOgger) stations, sampling air temperature and pressure, and 21 WXT weather stations, providing additional information on relative humidity, wind speed and precipitation. These stations were circularly distributed with a maximum radius of 30 km; suitable for the detection of CPs.

At all three supersites, Doppler wind LIDAR instruments were installed for vertically resolved wind measurements over heights of several hundred meters; ideal for observing LLJs. The supersites were located in Lindenberg (EG_L, 52.21°N, 14.13°E), Falkenberg (EG_F, 52.16°N, 14.14°E), and Birkholz (EG_B, 52.20°N, 14.19°E), with a distance of about ~6 km between each other. The flat area around EG_F and EG_B is agriculturally used, with the latter having trees in the vicinity. EG_L is located in a more complex area with buildings and a hill. The LIDAR in EG_F and EG_B operated in the gust mode, that is, allowing wind measurements with ~3 s temporal resolution (Steinheuer et al., 2022). The same gust mode was operated in EG_L, except for 01–10 June 2021 when the velocity azimuth display (VAD) method was used (Päschke et al., 2015). We compute 10 min averages of the winds retrieved from the LIDAR unless otherwise stated. Our analysis included only days when data for at least 50% of the profiles were available, with 72, 60 and 63 days available in EG_F, EG_L and EG_B.

We further used data for temporally continuous temperature profiling from a microwave radiometer (Löhnert et al., 2022) and tower measurements from 10 to 98 m in EG_F, and profiles from radiosondes (Kirsch et al., 2022) in EG_L. Radiosondes were launched every six hours, with additional launching at times of special events. For the analysis of the atmospheric stratification, we calculated the virtual potential temperature profiles and the Richardson Number (Ri) underneath the core of LLJs from the radiosondes and from standard instruments from the meteorological tower. Large Ri values ($Ri > 0.25$) imply that the stratification is stronger than shear-driven mixing. Unstable conditions and turbulent mixing are associated with negative Ri values (Han et al., 2021).

2.2. Automated Identifications

2.2.1. LLJ

Several automated detection methods for LLJ detection exist, for example, using relative (R. Banta et al., 2002; Tuononen et al., 2017; Wagner et al., 2019) or absolute (Andreas et al., 2000; R. Banta et al., 2002; Hallgren et al., 2020) criteria to identify sufficiently strong maxima in wind speed profiles. We adopt the method as in Luiz and Fiedler (2022) for comparability of the results. The algorithm uses a vertical shear in the wind speed stronger than -0.005 s^{-1} above the jet core for the characteristic nose of LLJs, paired with a minimum difference of 2 m s^{-1} between the jet core and the next minimum in the wind speed in the 500 m deep layer above the jet core. The jet core was defined as the first maximum in the wind speed in the lowest 500 m a.g.l..

Prior to the application of the LLJ detection algorithm, we smoothed the vertical profiles using moving averages every 5 measurement heights and obtained wind profiles with a vertical resolution of 26.5 m. The smoothing reduces the small scale and fast variability in the winds associated with turbulence. We then removed all detected LLJs shorter than 20 min since visual inspection showed that these were daytime profiles with strong turbulent

changes in the wind speed with height. The detection algorithm was applied in all profiles for which we had at least 75% of data between the surface and 1,000 ṁ a.g.l.. We connected individual LLJ detections, which were consecutive or had up to 20-min gaps in between, into one LLJ event. We therefore account for short intermittent mixing events during LLJs in the statistics.

2.2.2. Convective Cold Pools

Past studies identified convective Cold Pools (CP) using different data ranging from boundary layer towers (Goff, 1976; Kirsch et al., 2021), moving instruments aboard aircrafts and ships (de Szoeke et al., 2017; Terai & Wood, 2013), precipitation radars (Borque et al., 2020), model data (Heinold et al., 2013) and a combination of radar with LIDARS (Feng et al., 2015; Mueller & Carbone, 1987). In our study, we adapted the method from Kirsch et al. (2021) using 10 m temperature data from EG_F. The method defines a CP when a decrease in the temperature by more than 2 K in 20 min is measured. The first 10 min with a temperature difference by 0.5 K is defined as the front of the CP. The subsequent temperature decreases during the next hour are identified as part of the same CP event. The results from this method were validated against a list of CP events from FESSTVaL based on a multi-site identification method using the sensor network (Kirsch, 2022). Compared to the list, three CPs were not identified by our automated method, because of the lack of a sufficient temperature decrease in EG_F. We did not identify a LLJ for these cases. There were also four CPs that were missed by the algorithm, but had a LLJ signature. We therefore manually added these four CPs to our statistics and note that CP detection from single stations give conservative estimates of their statistics. All LLJs profiles that occurred at the same time as a CP were classified as CPLLJ*. All profiles from a LLJ event temporally connected to a CP, but not necessarily co-occurring with the CP, were classified as CPLLJ, that is, all CPLLJ* are included in the CPLLJ statistics.

3. Results

3.1. Statistics of LLJs

All supersites showed a similar frequency of occurrence for LLJs, with 20%–23% of all available profiles. When accounting only for nocturnal profiles, adopting a solar height below 20°, the LLJ frequency increased to 32%–34% of all profiles. The larger frequency of LLJs during the night period indicates a higher probability for forming a nocturnal LLJ (NLLJ) along with a stably stratified surface layer. To assess such NLLJs in more detail, we took all LLJs longer than six hours at night. From these NLLJ profiles in EG_F, 74% coincided with the occurrence of near-surface temperature inversions, measured by an average increase of the air temperature with height in the first 200 m a.g.l.. The average Ri value between the surface and the NLLJ core at 00 UTC during NLLJs was 1.4. Both the temperature inversion and the positive Ri are clear indicators of the nocturnal reduced frictional effects.

The co-occurrence of LLJs across the supersites depends on their duration. When a LLJs in EG_F occurred, we observed also a LLJ at the other two supersites in 75% of the cases. Restricting the analysis to events longer than 3 hr increased the LLJ co-occurrence to 84%. This is consistent with the perception that long-lived LLJs simultaneously occur over a larger spatial extent. Differently, when analyzing events shorter than 3 hr, the co-occurrence decreased to 47%. This is to be expected since short LLJs can be part of intermittent NLLJs or associated with density currents from CPs of smaller scale. For instance, 92% of the days had at least one LLJ detection, but events longer than one (three) hour were detected in 68% (40%) of the days in EG_F.

3.2. LLJs Associated With CPs

3.2.1. Statistical Assessment

The results of the joint detection of CPs and LLJs highlight that 6.8% of all LLJ profiles in EG_F were directly connected to a CP (CPLLJ). LLJs at the same time as the passage of the CP (CPLLJ*) add up to a fraction of 1.7%. From all CPLLJ (CPLLJ*) profiles in EG_F, we have seen in about 63% (28%) of the cases a simultaneous occurrence of a LLJ at the other two supersites. During CPLLJ detections in EG_F, we found a LLJ at the other two sites in 8% and at one other site in 20% of the cases. The average length of CPLLJs was about two hours. The median of the CP diameter during all the FESSTVaL campaign was 8.4 km (Kirsch, 2022). CPLLJs in a triangular area with a side length of about six km are therefore much shorter and local than NLLJs, owing to the fact that they migrate in space over time and have relatively short-lived driving mechanism. From the CP list in
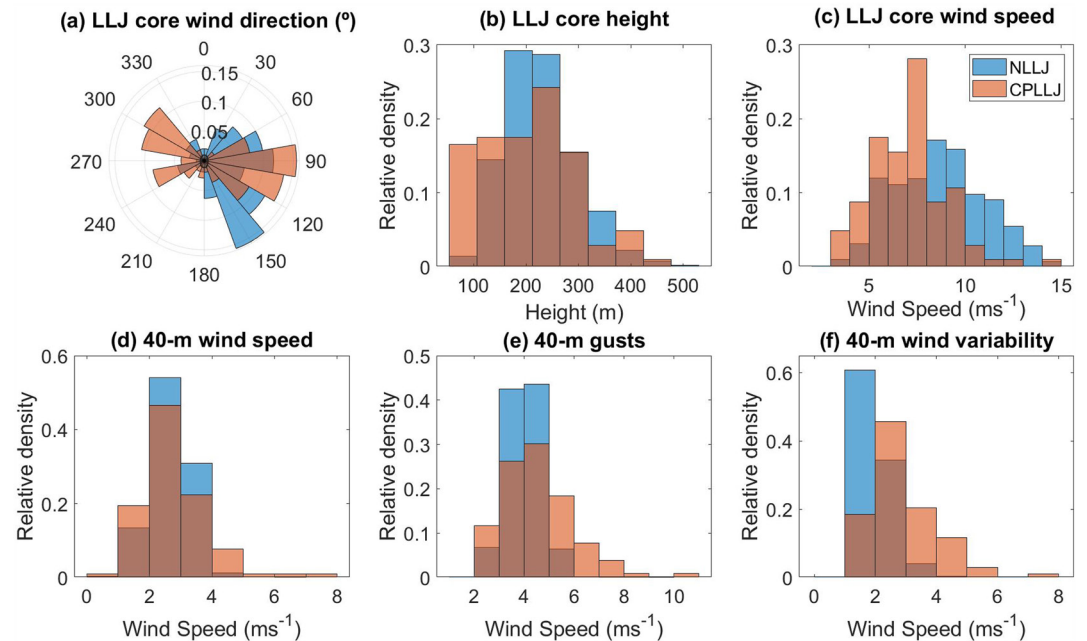
Figure 1. Relative density histograms of the wind during NLLJs and CPLLJs in EG_F. Shown are: (a) LLJ core wind direction, (b) LLJ core height, (c) LLJ core 10-min averaged wind speed, (d) 10-min averaged wind speed at 40 m, (e) 40 m wind gusts and (f) 40 m wind speed variability. Wind gusts are defined as the maximum 3s wind speed in 10-min intervals. The variability in (f) was calculated as the difference between the gust and the minimum wind speeds in the same 10-min intervals.

FESSTVaL, three CP occurred without a detected LLJ in EG_F and four CPs were not detected by the automatic method, but are identified by the CPLLJ detection. We can infer that, depending on the location and strength of the CP, they can affect regions away from their border.

CPLLJs occur under substantially different synoptic-scale conditions than NLLJs. The wind rose in Figure 1a shows that winds in the core of CPLLJs had two prevailing directions around Northwest and East, with easterlies being overall dominant. These directions are very different compared to the statistics for NLLJs that have primarily Southeasterlies in the core. While NLLJs are favored by anticyclonic weather patterns in Germany (Emeis, 2014; Luiz & Fiedler, 2022), our visual inspection of weather charts pointed to the influence of a low pressure system during CPLLJs (not shown). This result is consistent with the requirement of having a convective situation that allows for sufficient lift for the development of deep moist convection as origin of CPs.

CPLLJ were on average slightly weaker and lower than NLLJs. Figures 1b and 1c shows the distribution of the wind speed and the height of the jet cores. The mean wind speed in the core of CPLLJ (CPLLJ*) was 7.1 (7.4) m s^{-1} at a mean height of 207 (190) m. This is about 1.5 m s^{-1} less compared to the average wind speed in the core of NLLJs (8.6 m s^{-1}) and at a lower height by about 20 m (227 m). At the same time, the wind gusts in the core of CPLLJs were stronger, with speeds up to 17.5 m s^{-1} in EG_F exceeding the maximum of 15 m s^{-1} for NLLJs. Closer to the surface, the differences in the winds were larger than in the core. Analyzing 40 m wind speeds shows that winds during CPLLJs were on average weaker, but associated with stronger gusts compared to NLLJs (Figures 1d and 1e). The 10-min averaged differences between the maximum 3s gust and the minimum 3s wind speed were for instance 2.9 (1.9) m s^{-1} during CPLLJs (NLLJs) at 40 m a.g.l. (Figure 1f), indicative for the sharp wind variability of CPLLJs.

3.2.2. Temporal Development

Most CPLLJ appeared together with the CP front and were seen in our measurements for up to two hours after the front had passed. However, we observed three CPLLJ events longer than two hours with one such case during the afternoon of 29 June 2021. This CPLLJ event lasted for about six hours at EG_F and was recorded at all supersites (Figure 2). The CP reached EG_F around 14 UTC (16 LT), leading to jet-like profiles at all three supersites and strong winds with 10-min averages of up to 14 m s^{-1}. At EG_F, the CPLLJ started at the same time when the CP front arrived. The winds in the CPLLJ core were strong, for example, with gusts in the jet core (at 40 m) of up
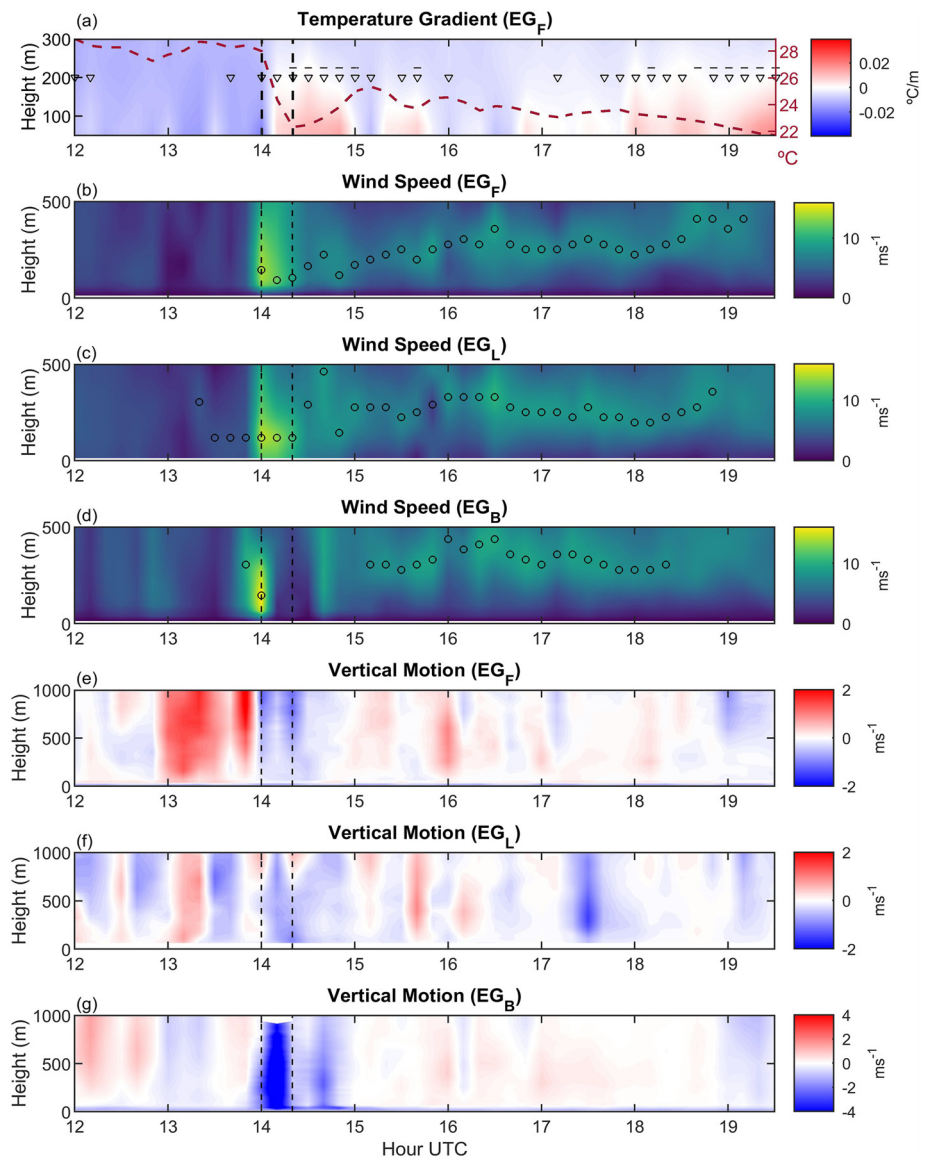
Figure 2. Temperature, stability metrics, and winds for the CPLLJ of 29 June 2021. Shown are time series (a) for (shading) the vertical gradient in air temperature from the microwave radiometer and (dashed line) the 10 m air temperature in EG_F, (b–d) the (shading) vertical profiles of wind speeds in EG_F, EG_L, and EG_B, and (e–g) profiles of vertical motion. The vertical dashed lines mark the start and end point of the CP detection. In a, ∇ and $-$ mark the times with above-threshold Ri and positive vertical gradients in the virtual potential temperature calculated from the meteorological tower between 10 and 80 m as indicators for near-surface stable conditions. In b–d, black circles mark the automated detection of LLJs.

to 21 (13) m s^{-1} in EG_B. The CPLLJ persisted until about 19 UTC (21 LT) at EG_L and EG_F. In EG_B, the density current started slightly earlier due to the geographical position of the site upwind from the other two sites. There, the CPLLJ development was interrupted by a break of about one hour after the CP had passed due to stronger precipitation and a second downdraft delaying the local formation of the CPLLJ (Figure 2g). This difference is due to local influences on the winds since the other two sites had a continuous detection of a CPLLJ over time. We also see changing heights for the core of the CPLLJ, particularly in the first hour after the CP passage. This behavior is possibly connected to gravity waves in the wake of the migrating cold pool, for example, known from other density currents (Udina et al., 2013) and consistent with dipoles of upward and downward motion (Figure 2e–2g). At EG_L, there was also a weak LLJ signature up to about 40 min ahead of the CP, possibly connected to upslope winds at the hill due to the strong daytime heating, reflected by a 2 m air temperature of 28°C before the arrival of the CP.
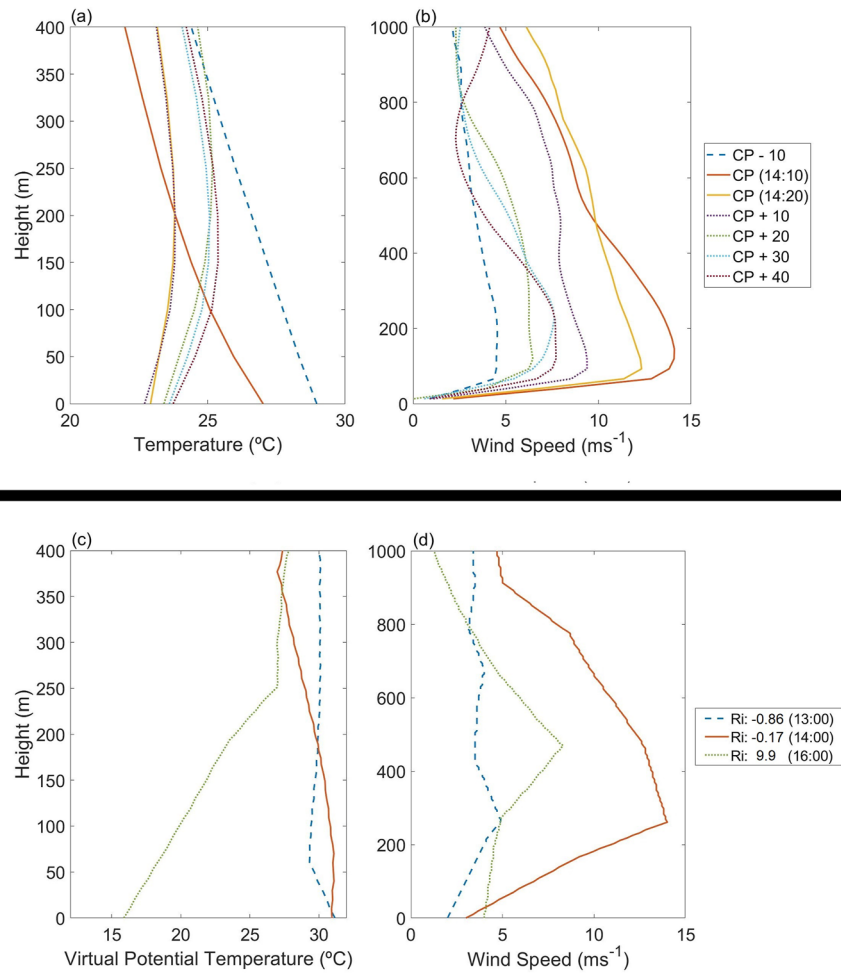
Figure 3. Vertical profiles during the CPLLJ of 29 June 2021 in Falkenberg at the top and Lindenberg at the bottom. Shown are vertical profiles of (a–b) temperature from the microwave radiometer and wind speed from the Doppler wind LIDAR in EG_F, (c–d) virtual potential temperature with the vertically averaged Ri and wind speed from the radiosondes in EG_L. CP in a,b are the 10-min averaged profiles at the time of the automatically identified CP, with ± indicating the time difference relative to the CP in minutes. All times are in UTC.

A CP can favor the formation of a surface-temperature inversion that results in a LLJ formation similar to NLLJs. The CP arrived in EG_F around 14 UTC on 29 June 2021, visible as rapid reduction in the 10 m air temperature by 5.7°C within 20 min (Figures 2a and 3a). At the same time when the density current reached the site, a CPLLJ* profile occurred. The CPLLJ* shows the strongest wind speeds around 100 m a.g.l. with gusts of up to 17 m s⁻¹ at EG_F. The vertical profile of the wind speed has already the characteristic nose-like shape for a LLJ at all three sites when the CP front arrives (Figure 2b). At that time the temperature profile is, however, still indicating unstable stratification (Figures 3a and 3c). Ten minutes after the passage of the leading edge of the CP, a temperature inversion is first seen, the winds slacken throughout the profile and CPLLJs profiles are identified (Figure 2). Because this development begins in the daytime convective boundary layer (16 LT), it is a clear indicator that CPs can contribute to building a surface temperature inversion. In the case assessed here, the CP initially cooled all layers between the surface and up to at least 400 m a.g.l., leading to a stronger cooling of the layers closest to the surface (Figure 3a). Ten minutes later, the levels below 200 m a.g.l. continued to cool, forming a temperature inversion as one would typically expect much later in the transition to night.

The formation of the temperature inversion reduced the frictional coupling of the winds in some distance to the surface in the wake of the CP, allowing LLJs to form already during the day with a mechanism similar to NLLJs. That change in stratification is seen ten minutes after the CP front, for example, as inversion in the air temperature

over the lowest 200 m in EG_F (Figure 2a). The newly formed CPLLJ in EG_F is continuously seen in the measurements until 19 UTC. During the CPLLJ lifetime, several intermittent mixing events occurred indicated by the change in the vertical stratification and below-threshold Ri, particularly in the evening transition between 16 and 18 UTC, that is, two to four hours after the CP front. After 18 UTC, the nocturnal radiative cooling sufficiently strengthens the surface inversion again to increase Ri. The development of low-level stratification including the height of the CPLLJs is clearly seen in the vertical profiles for virtual potential temperature from radiosondes in EG_L (Figures 3c and 3d). One hour ahead of the CP, the boundary layer had the typical daytime profile with unstable conditions close to the surface and a neutral stratification in the well-mixed layer with light winds throughout the boundary layer (13 UTC, 15 LT). At the time of the CP arrival in EG_L and EG_F (14 UTC, 16 LT), the virtual potential temperature decreased with height, indicative for convective mixing and a strong LLJ appears, with 14 m s^{-1} in the core around 260 m a.g.l.. The virtual potential temperature profile shows a stably stratified surface layer in the wake of the CP (16 UTC, 18 LT) with a strong inversion between the surface up to 250 m a.g.l.. At that time, a CPLLJ is seen with a core around 500 m a.g.l. near the top of the surface inversion, in agreement with the LIDAR measurements. The Ri values support these findings with $Ri = -0.86$ and $Ri = -0.17$ at 13 and 14 UTC indicative for vertical mixing, and $Ri = 9.9$ at 16 UTC that is characteristic for a stable stratification. The CPLLJ ended around 19 UTC (21 LT), thus around the time when NLLJ development would typically begin. In fact, NLLJs were mostly detected after 19 UTC during FESSTVaL. We suspect that the CPLLJ could have continued in the course of the night if no perturbation would have occurred. Although some periods of atmospheric stability were identified in the night after the CP event, the influence of a low pressure system prevented a sufficient reduction of the frictional coupling to the surface that would be needed for a NLLJ.

4. Discussion and Conclusion

The present study shows the first observational assessment of convectively generated cold pools (CP) as driving mechanism for low-level jets (LLJ) based on unique measurements in Central Europe. We provide observational evidence for how a CP can contribute to the formation of a surface-temperature inversion that allows a LLJ to develop in the wake of a CP. The connection of LLJs and CP events was earlier only documented in convection-permitting simulations over Africa (Heinold et al., 2013), describing dust storms simultaneously connected to LLJs and CPs. Heinold et al. (2013) inferred that aged cold pools glide up over a radiatively formed stable surface layer, triggering LLJ formation over a large area due to the locally induced pressure gradient. Our observational results highlight that a cold pool itself can help to form the surface inversion needed for a prolonged LLJ development. The atmosphere initially begun to cool from the surface to at least 400 m a.g.l. with the arrival of the CP. The temperature inversion developed behind the leading edge of the CP, when the air below 200 m a.g.l. continued to cool. Since this development occurred during daytime when radiative cooling does not dominate the temperature development, it points to CPs as trigger for the formation of a surface inversion. The associated reduced frictional coupling of the wind with the surface allowed the generation of LLJs in the wake of the CP already during daytime and not unlike the mechanism of nocturnal LLJs. We did not observe a continuous turning of the wind for LLJs connected to cold pools (CPLLJ), but this is also not the case for most nocturnal LLJs at the site due to non-stationary conditions. The strongest near-surface temperature inversion is seen at the beginning of CPLLJ, namely up to one hour after the CP front. Due to the later weaker stability, the winds in the CPLLJ core were weaker and there was more vertical mixing than earlier during the event.

LLJs connected to cold pools (CPLLJ) comprised 6.8% of the LLJ profiles in summer 2021. The average lifetime of CPLLJs was two hours. Due to their low frequency of occurrence, CPLLJs do not strongly influence LLJ climatologies in regions where convective downdrafts play a minor role, but some of their characteristics, for example, stronger gusts and wind variability compared to nocturnal LLJs, can have adverse impacts, for example, for wind power production (Kalverla et al., 2019). The lower height and gusty winds associated with CPLLJs impacts wind parks feeding electricity into the transmission grid that needs to keep a stable frequency within a tight range to avoid blackouts. Rapid temporal changes in wind speeds like during CPLLJs can lead to power fluctuations. These can be technically balanced, but need to be known, for example, from forecasts and from climatological assessments. To that end, we compared the observed CPLLJs against ERA5 reanalysis data and found that none of the CPLLJs were simulated (not shown). Hence, a driving mechanism of LLJs is entirely missing. There is good reason to believe that this is also true for other weather and climate models with parameterized convection, for example, indicated by the challenge to simulate clouds and circulation (Bony et al., 2015). Simulating CPLLJ is important due to their momentum transfer, for example, relevant for storm damages and

exchange processes between the atmosphere and the underlying land or ocean, as well as for pollutant transport and more broadly their interactions with meso-scale dynamical processes. Although CPLLJ are rare in Germany, they can be much larger and more frequent elsewhere, for example, in West Africa (Heinold et al., 2013). Future research might advance our understanding of CPLLJ statistics and their impacts, when more storm-resolving simulations become available.

Data Availability Statement

All FESSTVaL data is available in the SAMD archive found at https://www.cen.uni-hamburg.de/en/icdc/data/atmosphere/samd-st-datasets/samd-st-fesstval.html. The LIDAR data using gust mode can be found at https://doi.org/10.25592/uhhfdm.11227 and using VAD mode at https://www.fdr.uni-hamburg.de/record/11394. The microwave radiometer observations can be found at https://doi.org/10.25592/uhhfdm.10198, the radiosondes profiles can be found at https://www.fdr.uni-hamburg.de/record/10279 and the data from the network observations by APOLLO and WXT weather stations can be found at https://www.fdr.uni-hamburg.de/record/10179.

References

Andreas, E. L., Claffy, K. J., & Makshtas, A. P. (2000). Low-level atmospheric jets and inversions over the western Weddell Sea. *Boundary-Layer Meteorology*, *97*(3), 459–486. https://doi.org/10.1023/A:1002793831076

Angevine, W. M., Tjernström, M., & Žagar, M. (2006). Modeling of the coastal boundary layer and pollutant transport in New England. *Journal of Applied Meteorology and Climatology*, *45*(1), 137–154. https://doi.org/10.1175/jam2333.1

Banta, R., Newsom, R. K., Lundquist, J. K., Pichugina, Y. L., Coulter, R. L., & Mahrt, L. (2002). Nocturnal low-level jet characteristics over Kansas during cases-99. *Boundary-Layer Meteorology*, *105*(2), 221–252. https://doi.org/10.1023/A:1019992330866

Banta, R. M., Darby, L. S., Fast, J. D., Pinto, J. O., Whiteman, C. D., Shaw, W. J., & Orr, B. W. (2004). Nocturnal low-level jet in a mountain basin complex. part i: Evolution and effects on local flows. *Journal of Applied Meteorology and Climatology*, *43*(10), 1348–1365. https://doi.org/10.1175/jam2142.1

Beyrich, F. (1994). Sodar observations of the stable boundary layer height in relation to the nocturnal low-level jet. *Meteorologische Zeitschrift. Neue Folge (Berlin)*, *3*(1), 29–34. https://doi.org/10.1127/metz/3/1994/29

Blackadar, A. K. (1957). Boundary layer wind maxima and their significance for the growth of nocturnal inversions. *Bulletin of the American Meteorological Society*, *38*(5), 283–290. https://doi.org/10.1175/1520-0477-38.5.283

Bony, S., Stevens, B., Frierson, D. M., Jakob, C., Kageyama, M., Pincus, R., et al. (2015). Clouds, circulation and climate sensitivity. *Nature Geoscience*, *8*(4), 261–268. https://doi.org/10.1038/ngeo2398

Borque, P., Nesbitt, S. W., Trapp, R. J., Lasher-Trapp, S., & Oue, M. (2020). Observational study of the thermodynamics and morphological characteristics of a midlatitude continental cold pool event. *Monthly Weather Review*, *148*(2), 719–737. https://doi.org/10.1175/mwr-d-19-0068.1

Chen, G. T.-J., Wang, C.-C., & Lin, L.-F. (2006). A diagnostic study of a retreating mei-yu front and the accompanying low-level jet formation and intensification. *Monthly Weather Review*, *134*(3), 874–896. https://doi.org/10.1175/mwr3099.1

Chen, R., & Tomassini, L. (2015). The role of moisture in summertime low-level jet formation and associated rainfall over the East Asian monsoon region. *Journal of the Atmospheric Sciences*, *72*(10), 3871–3890. https://doi.org/10.1175/jas-d-15-0064.1

Corrêa, P. B., Dias-Júnior, C. Q., Cava, D., Sörgel, M., Botía, S., Acevedo, O., et al. (2021). A case study of a gravity wave induced by amazon forest orography and low level jet generation. *Agricultural and Forest Meteorology*, *307*, 108457. https://doi.org/10.1016/j.agrformet.2021.108457

de Szoeke, S. P., Skyllingstad, E. D., Zuidema, P., & Chandra, A. S. (2017). Cold pools and their influence on the tropical marine boundary layer. *Journal of the Atmospheric Sciences*, *74*(4), 1149–1168. https://doi.org/10.1175/jas-d-16-0264.1

Drager, A. J., & van den Heever, S. C. (2017). Characterizing convective cold pools. *Journal of Advances in Modeling Earth Systems*, *9*(2), 1091–1115. https://doi.org/10.1002/2016ms000788

Emeis, S. (2014). Wind speed and shear associated with low-level jets over northern Germany. *Meteorologische Zeitschrift*, *23*(3), 295–304. https://doi.org/10.1127/0941-2948/2014/0551

Feng, Z., Hagos, S., Rowe, A. K., Burleyson, C. D., Martini, M. N., & de Szoeke, S. P. (2015). Mechanisms of convective cloud organization by cold pools over tropical warm ocean during the AMIE/DYNAMO field campaign. *Journal of Advances in Modeling Earth Systems*, *7*(2), 357–381. https://doi.org/10.1002/2014ms000384

Goff, R. C. (1976). Vertical structure of thunderstorm outflows. *Monthly Weather Review*, *104*(11), 1429–1440. https://doi.org/10.1175/1520-0493(1976)104<1429:vsoto>2.0.co;2

Gutierrez, W., Araya, G., Kiliyanpilakkil, P., Ruiz-Columbie, A., Tutkun, M., & Castillo, L. (2016). Structural impact assessment of low level jets over wind turbines. *Journal of Renewable and Sustainable Energy*, *8*(2), 023308. https://doi.org/10.1063/1.4945359

Hallgren, C., Arnqvist, J., Ivanell, S., Körnich, H., Vakkari, V., & Sahlée, E. (2020). Looking for an offshore low-level jet champion among recent reanalyses: A tight race over the Baltic Sea. *Energies*, *13*(14), 3670. https://doi.org/10.3390/en13143670

Han, Y., Yang, Q., Liu, N., Zhang, K., Qing, C., Li, X., et al. (2021). Analysis of wind-speed profiles and optical turbulence above gaomeigu and the Tibetan plateau using ERA5 data. *Monthly Notices of the Royal Astronomical Society*, *501*(4), 4692–4702. https://doi.org/10.1093/mnras/staa2960

Heinold, B., Knippertz, P., Marsham, J., Fiedler, S., Dixon, N., Schepanski, K., et al. (2013). The role of deep convection and nocturnal low-level jets for dust emission in summertime West Africa: Estimates from convection-permitting simulations. *Journal of Geophysical Research: Atmospheres*, *118*(10), 4385–4400. https://doi.org/10.1002/jgrd.50402

Hohenegger, C., Ament, F., Beyrich, F., Löhnert, U., Rust, H., Bange, J., et al. Fesstval: The field experiment on submesoscale spatio-temporal variability in lindenberg. *Bulletin of the American Meteorological Society*. (in review).

Kalverla, P. C., Duncan, J. B., Steeneveld, G. J., & Holtslag, A. A. (2019). Low-level jets over the north sea based on ERA5 and observations: Together they do better. *Wind Energy Science*, *4*(2), 193–209. https://doi.org/10.5194/wes-4-193-2019

Kirsch, B. (2022). *Illuminating convective cold pools with a dense station network* (PhD thesis). Universität Hamburg. https://doi.org/10.17617/2.3432702

Kirsch, B., Ament, F., & Hohenegger, C. (2021). Convective cold pools in long-term boundary layer mast observations. *Monthly Weather Review*, *149*(3), 811–820. https://doi.org/10.1175/mwr-d-20-0197.1

Kirsch, B., Stiehle, B., Löhnert, U., & Ament, F. (2022). Radiosonde profile measurements during fesstval 2021. Universität Hamburg. https://doi.org/10.25592/uhhfdm.10279

Lampert, A., Bernalte Jimenez, B., Gross, G., Wulff, D., & Kenull, T. (2016). One-year observations of the wind distribution and low-level jet occurrence at Braunschweig, North German Plain. *Wind Energy*, *19*(10), 1807–1817. https://doi.org/10.1002/we.1951

Li, X., & Du, Y. (2021). Statistical relationships between two types of heavy rainfall and low-level jets in south China. *Journal of Climate*, *34*(21), 8549–8566. https://doi.org/10.1175/jcli-d-21-0121.1

Löhnert, U., Knist, C., Böck, T., & Pospichal, B. (2022). Microwave radiometer observations during fesstval 2021. Universität Hamburg. https://doi.org/10.25592/uhhfdm.10198

Lu, W., & Zhong, S. (2014). A numerical study of a persistent cold air pool episode in the salt lake valley, Utah. *Journal of Geophysical Research: Atmospheres*, *119*(4), 1733–1752. https://doi.org/10.1002/2013jd020410

Luiz, E. W., & Fiedler, S. (2022). Spatiotemporal observations of nocturnal low-level jets and impacts on wind power production. *Wind Energy Science*, *7*(4), 1575–1591. https://doi.org/10.5194/wes-7-1575-2022

Mueller, C. K., & Carbone, R. E. (1987). Dynamics of a thunderstorm outflow. *Journal of the Atmospheric Sciences*, *44*(15), 1879–1898. https://doi.org/10.1175/1520-0469(1987)044<1879:doato>2.0.co;2

Päschke, E., Leinweber, R., & Lehmann, V. (2015). An assessment of the performance of a 1.5 μm Doppler lidar for operational vertical wind profiling based on a 1-year trial. *Atmospheric Measurement Techniques*, *8*(6), 2251–2266. https://doi.org/10.5194/amt-8-2251-2015

Schepanski, K., Tegen, I., Todd, M. C., Heinold, B., Bönisch, G., Laurent, B., & Macke, A. (2009). Meteorological processes forcing Saharan dust emission inferred from MSG-SEVIRI observations of subdaily dust source activation and numerical models. *Journal of Geophysical Research*, *114*(D10), D10201. https://doi.org/10.1029/2008JD010325

Shapiro, A., & Fedorovich, E. (2010). Analytical description of a nocturnal low-level jet. *Quarterly Journal of the Royal Meteorological Society*, *136*(650), 1255–1262. https://doi.org/10.1002/qj.628

Sisterson, D. L., & Frenzen, P. (1978). Nocturnal boundary-layer wind maxima and the problem of wind power assessment. *Environmental Science & Technology*, *12*(2), 218–221. https://doi.org/10.1021/es60138a014

Steinheuer, J., Detring, C., Beyrich, F., Löhnert, U., Friederichs, P., & Fiedler, S. (2022). A new scanning scheme and flexible retrieval for mean winds and gusts from Doppler lidar measurements. *Atmospheric Measurement Techniques*, *15*(10), 3243–3260. https://doi.org/10.5194/amt-15-3243-2022

Terai, C., & Wood, R. (2013). Aircraft observations of cold pools under marine stratocumulus. *Atmospheric Chemistry and Physics*, *13*(19), 9899–9914. https://doi.org/10.5194/acp-13-9899-2013

Tuononen, M., O'Connor, E. J., Sinclair, V. A., & Vakkari, V. (2017). Low-level jets over Utö, Finland, based on Doppler lidar observations. *Journal of Applied Meteorology and Climatology*, *56*(9), 2577–2594. https://doi.org/10.1175/jamc-d-16-0411.1

Udina, M., Soler, M., Viana, S., & Yagüe, C. (2013). Model simulation of gravity waves triggered by a density current. *Quarterly Journal of the Royal Meteorological Society*, *139*(672), 701–714. https://doi.org/10.1002/qj.2004

Van de Wiel, B. J. H., Moene, A. F., Steeneveld, G. J., Baas, P., Bosveld, F. C., & Holtslag, A. A. M. (2010). A conceptual view on inertial oscillations and nocturnal low-level jets. *Journal of the Atmospheric Sciences*, *67*(8), 2679–2689. https://doi.org/10.1175/2010JAS3289.1

Wagner, D., Steinfeld, G., Witha, B., Wurps, H., & Reuder, J. (2019). Low level jets over the southern North Sea. *Meteorologische Zeitschrift*, *28*(5), 389–415. https://doi.org/10.1127/metz/2019/0948

Whiteman, C. D., Zhong, S., Shaw, W. J., Hubbe, J. M., Bian, X., & Mittelstadt, J. (2001). Cold pools in the Columbia basin. *Weather and Forecasting*, *16*(4), 432–447. https://doi.org/10.1175/1520-0434(2001)016<0432:cpitcb>2.0.co;2

Ziemann, A., Galvez Arboleda, A., & Lampert, A. (2020). Comparison of wind Lidar data and numerical simulations of the low-level jet at a grassland site. *Energies*, *13*(23), 6264. https://doi.org/10.3390/en13236264